Transient ion resonance instability

J. Fajans
Department of Physics, University of California, Berkeley, Berkeley, California 94720

(Received 22 February 1993; accepted 12 April 1993)

A trapped pure electron plasma column can be unstable if the plasma column is contaminated by a small number of oppositely charged ions. This instability was analyzed by Levy, Daugherty, and Buneman [Phys. Fluids, **12**, 2616 (1969)] for the case of trapped ions. The instability is analyzed here for the case of untrapped ions. The analysis is inherently nonlinear, and growth results from averaging over the ion initial conditions. Several significant differences exist between the two cases, including, for the latter, growth over a much broader parameter region and linear (secular) rather than exponential growth. The predictions of the analysis are compared to the results from a recent experiment on the instability.

I. INTRODUCTION

A trapped pure electron plasma column can be unstable if the plasma column is contaminated by a small number of oppositely charged ions. This instability, named the ion resonance instability by Levy, Daugherty, and Buneman[1] manifests itself by the gradual displacement of the plasma column from the central axis of the electron trap. Growth takes place when the frequency of the off-axis diocotron oscillation[2] of the electron column is close to the frequency of the ion oscillations through the potential well formed by the electron column. Maximum growth occurs when these two frequencies are approximately equal, and growth persists for arbitrarily small ion densities.

Whether deliberately or inadvertently, several past, current, and planned non-neutral plasma experiments are partially neutralized.[3–6] For example, several planned experiments on antihydrogen production require the addition of protons to trapped positron plasmas. The instability is suspected to be the dominant loss mechanism in toroidal experiments.[7–9] In general, without both very low background pressures and low electron temperatures, ions will always be present in any electron trap.

The instability has recently been observed in a linear, finite length, Penning/Malmberg electron trap.[6] In these experiments the contaminant ions are created by ionization of the background gas by the hot electrons in the plasma column. Since the ionization process is unlikely to significantly change the kinetic energy of the relatively massive background gas atoms, the newly created ions will initially drift with only their thermal velocity. Ions are not axially confined in electron Penning traps, so the ions axially drift out of the system on a time scale τ. This transit time τ is too short and the ion density is too low for the classic bunching instability postulated by Levy *et al.* to be relevant. I will show that the instability is instead caused by an initial condition effect. This new theory correctly predicts that the instability occurs over a wide range of parameters, that the instability can grow linearly ($\propto t$) rather than exponentially ($\propto \exp \Gamma t$), and that it gives plausible estimates of the growth rate.

The electron trap employs a strong axial magnetic field $\mathbf{B} = B\hat{z}$ to radially confine the electrons inside a coaxial, conducting, confinement cylinder. Negatively biased cylinders placed at both ends of the confinement cylinder provide axial confinement. Similar traps are described in the literature.[10] The electron column produces an inwardly directed electric field $\mathbf{E} = E\hat{r}$ that causes the electron column to $\mathbf{E}\times\mathbf{B}$ rotate around its central axis. [Note that in this paper I will use cylindrical $(\hat{r},\hat{\theta},\hat{z})$ coordinates, rectangular $(\hat{x},\hat{y},\hat{z})$ coordinates, and several shifted and rotating coordinates; a carat over a symbol indicates that it is a unit vector.]

If the electron column is displaced from the central axis by a distance R_D, the surrounding conducting cylinder forms an oppositely charged image at radius a^2/R_D, where a is the radius of the conducting cylinder. This image charge acts back upon the electron column to produce an azimuthal drift of the entire column. This drift, called a diocotron mode, causes the electron column to rotate around the trap axis with frequency ω_D. For a column of uniform density n_0, radius b, displaced a small distance from the trap center, this frequency is $\omega_D = en_0b^2/2\epsilon_0Ba^2$, where $-e$ is the charge on the electron. Thus the typical motion of an electron in the trap consists of a fast rotation around the electron column axis superimposed on a slow drift around the trap axis. The electrons also bounce from one end of the trap to the other; however, this axial motion is much faster than the radial and azimuthal drifts. Consequently the axial bounce adiabatic invariant is conserved, and, since the plasma length is also constant, the total axial kinetic energy is invariant and will henceforth be ignored. Because the electrons are strongly magnetized their kinetic energy is insignificant compared to their electrostatic energy. In the absence of ions, the electron column energy per unit length,

$$U_e = -\frac{1}{2}\int_0^a r\,dr \int_0^{2\pi} d\theta\, en(r)\varphi(r), \tag{1}$$

is conserved. Here $\varphi(r)$ is the electrostatic potential. Since the system boundaries are azimuthally symmetric, the electron column angular momentum per unit length,

$$\mathbf{L}_e = -\frac{eB}{2}\int_0^a r\,dr \int_0^{2\pi} d\theta\, r^2 n(r) \tag{2}$$

 0899-8221/93/5(9)/3127/9/$6.00

is also conserved. Note that the electron kinetic angular momentum is insignificant compared to the canonical angular momentum.[11]

If the quantities U_e and $\mathbf{L}_e$ were absolutely invariant, the amplitude of the diocotron mode could never increase and the ion resonance instability would not occur. However, the continuous production of ions can change these quantities. I will show that as the ions move through the electron column, their energy U_i and angular momentum $\mathbf{L}_i$ vary. Because the total energy and angular momentum are conserved, the difference between the U_i and $\mathbf{L}_i$ that the ions carry out with them when they escape from the trap and the U_i and $\mathbf{L}_i$ that the ions posses when they are born must be transferred to the electron column. The change in U_i and $\mathbf{L}_i$ depends on the initial conditions, and is different for each ion. However, the average change is always positive, and the instability will grow, albeit sometimes at a very low level, for all system parameters.

In Sec. II of this paper, I find the ion equation of motion and find general expressions for the changes in the ion energy and angular momentum as the ion propagates through the plasma column. In Sec. III, these changes are related to changes in the electron column displacement. In Sec. IV, I analyze the ion orbits for the specific case of a flat-top electron column density distribution, and find approximate expressions for the instability growth rate in various limits. In Sec. V, these expressions are tested by comparing their predictions to the results of numeric simulations. The simulation results are also compared to experimental data.[6] In the concluding section, the successes and limitations of this theory are summarized. The range of experiments subject to the transient ion resonance instability is also briefly discussed. Finally, in the Appendix, I extend Levy *et al.*'s theory to include initial conditions and show that their theory is inapplicable to the experimental results.[6]

II. ION ORBITS

The ions are attracted to the center of the electron plasma column by the plasma electric field $\mathbf{E}$, but are prevented from falling into the exact center by the axial magnetic field $\mathbf{B}$. The ion equation of motion is most simply expressed using normalized quantities (denoted by overbars):

$$\frac{d^2\bar{\mathbf{x}}}{d\bar{t}^2}=\bar{\mathbf{E}}+\lambda^{1/2}\bar{\mathbf{v}}\times\hat{z}. \tag{3}$$

Here distances and velocities are normalized by the conducting cylinder radius a such that $\bar{\mathbf{x}}=\mathbf{x}/a$, $\bar{\mathbf{v}}=\mathbf{v}/a$, time is normalized as $\bar{t}=(n_0e^2/2\epsilon_0m_i)^{1/2}t$, electric fields are normalized as $\bar{\mathbf{E}}=(2\epsilon_0/n_0ea)\mathbf{E}$, and m_i is the ion mass. The electric fields depend on the position of the electron column, which depends on the diocotron frequency $\bar{\omega}_D$. In normalized coordinates this frequency is $\bar{\omega}_D=\bar{b}^2/\lambda^{1/2}$. With these normalizations, the ion orbits depend on the system parameters only through $\lambda=2\epsilon_0B^2/n_0m_i$ and $\bar{b}$. Hence, aside from a trivial scale factor in $\bar{t}$, the ion dynamics are completely governed by the ion magnetization parameter λ and the column radius $\bar{b}$.[1]

The normalized ion energy is

$$\bar{U}_i=\tfrac{1}{2}|\bar{\mathbf{v}}|^2+\bar{\varphi}, \tag{4}$$

where the electron column potential is normalized as $\bar{\varphi}=(2\epsilon_0/n_0e)\varphi$. Ultimately I need to find the change in $\bar{U}_i$. Taking the total derivative of Eq. (4) gives

$$\frac{d\bar{U}_i}{d\bar{t}}=\frac{\partial\bar{\varphi}}{\partial\bar{t}}, \tag{5}$$

where I have used Eq. (3) and $\bar{\mathbf{E}}=-\bar{\nabla}\bar{\varphi}$. In the lab frame the potential $\bar{\varphi}$ is a function of the electron column position. However, if I ignore the gradual increase in the diocotron radius as the instability progresses, the column is stationary in a frame rotating at the diocotron frequency $\bar{\omega}_D$ and, without loss of generality, can be assumed to be at position $(\bar{x}_D=\bar{R}_D,\bar{y}_D=0)$. In this frame Eq. (5) simplifies to

$$\frac{d\bar{U}_i}{d\bar{t}}=\bar{\omega}_D(\bar{\mathbf{x}}_D\times\bar{\mathbf{E}}_D)\hat{z}, \tag{6}$$

where the subscript D denotes quantities in the rotating frame.

In the lab frame the ion angular momentum is

$$\mathbf{L}_i=m_i\mathbf{x}\times\mathbf{v}+\frac{eB}{2}|\mathbf{x}|^2\hat{z}. \tag{7}$$

With the normalization $\bar{L}_i=(2\epsilon_0/m_in_0e^2a^4)^{1/2}L_i$, Eq. (7) reduces to

$$\bar{L}_i\hat{z}=\bar{\mathbf{x}}\times\bar{\mathbf{v}}+\tfrac{1}{2}\lambda^{1/2}|\bar{\mathbf{x}}|^2\hat{z}. \tag{8}$$

Taking the total derivative of this equation and using Eq. (3) yields

$$\frac{d\bar{L}_i}{d\bar{t}}=(\bar{\mathbf{x}}\times\bar{\mathbf{E}})_{\hat{z}}=(\mathbf{x}_D\times\mathbf{E}_D)_{\hat{z}}, \tag{9}$$

where the transformation to the rotating diocotron frame is permitted because $\bar{L}_i$ is normal to the rotation plane. Integration of Eqs. (6) and (9) along the ion orbits gives the change in ion energy $\Delta\bar{U}_i$ and angular momentum $\Delta\bar{L}_i$. Remarkably, these quantities are related by the constant $\bar{\omega}_D$. This result can be anticipated,[12] however, by transforming the ion Hamiltonian into the diocotron frame; $H_D=H-\bar{\omega}_D\bar{L}_i$. Since the Hamiltonian is time invariant in this frame, $0=\Delta H_D=\Delta H-\bar{\omega}_D\Delta\bar{L}_i$, so $\Delta\bar{U}_i=\Delta H=\bar{\omega}_D\Delta\bar{L}_i$.

III. THE ELECTRON COLUMN

The electron column energy and angular momentum are determined by the diocotron radius $\bar{R}_D$ and column radius $\bar{b}$. In principle, both $\bar{R}_D$ and $\bar{b}$ might need to be adjusted to respond to changes induced by $\Delta\bar{U}_i$ and $\Delta\bar{L}_i$. However, by ignoring[11] the electron kinetic terms in the expressions for the column energy and angular momentum [Eqs. (1) and (2)], I have limited the response of the

electrons to $\mathbf{E}\times\mathbf{B}$ flow. Such flow is area preserving; consequently the column radius cannot expand. The electron density can be modeled as

$$\bar{n}_e(\tilde{r}) = \bar{n}_0 f(\tilde{r}/\bar{b}), \tag{10}$$

where $f(u)$ is an arbitrary function constrained to equal zero at the confining cylinder wall, and $\bar{n}_0 = n_0 a^2$ is the scaled density. The radius $\tilde{r}$ is measured from the center of the plasma; consequently the column profile is assumed to remain unchanged even when the column is off center by $\bar{R}_D$. With this model, the number of electrons per unit length equals $N_e = \pi \bar{n}_0 \bar{b}^2 I_1$, where $I_1 = 2\int_0^\infty du\, u f(u)$, and is self-evidently independent of $\bar{b}$. For a constant density column of radius $\bar{b}$, $I_1 = 1$. Note that the upper limit of this integral has been safely extended from the wall radius to infinity without changing I_1 because the function $f(u)$ is constrained to be zero at the wall.

Substitution of Eq. (10) into Eq. (2) yields the angular momentum per unit length of the electron column:

$$\bar{L}_e = -\tfrac{1}{2}\pi \bar{n}_0 \bar{b}^2 \lambda^{1/2}(\bar{R}_D^2 I_1 + \tfrac{1}{2}\bar{b}^2 I_3), \tag{11}$$

where $I_3 = 4\int_0^\infty du\, u^3 f(u)$. The differential of this expression is easily obtained:

$$\Delta \bar{L}_e = -\pi \bar{n}_0 \bar{b}^2 \lambda^{1/2} \bar{R}_D I_1 \Delta \bar{R}_D. \tag{12}$$

System angular momentum conservation requires that $\Delta \bar{L}_e = -\Delta \bar{L}_i$; thus

$$\Delta \bar{R}_D = \frac{\Delta \bar{L}_i}{\pi \bar{n}_0 \bar{b}^2 \lambda^{1/2} I_1 \bar{R}_D} \tag{13}$$

is the change induced in the diocotron radius by a single ion. This change in $\bar{R}_D$ is small, and the ion transit time τ is small compared to the growth time. Consequently, each ion acts independently, and $d\bar{R}_D/dt$ equals the average value of $\Delta \bar{R}_D$ times the ion production rate per unit length $\mathcal{R}$. Rather than model the details of the ionization process, I simply observe that the production rate is $\mathcal{R} = N_i/\tau$, where N_i is the number of ions per unit length. If I further assume that the number of ions is proportional to the number of electrons N_e, then $N_i = \pi \bar{n}_i \bar{b}^2 I_1$. Using this expression with Eq. (13) gives

$$\frac{d\bar{R}_D}{dt} = \frac{\bar{n}_i}{\bar{n}_0 \tau} \frac{1}{\lambda^{1/2}\bar{R}_D} \langle \Delta \bar{L}_i \rangle, \tag{14}$$

where $\langle \Delta \bar{L}_i \rangle$ is the average change in the ion angular momentum. It can be shown that the change in the electron column energy [Eq. (1)] is exactly compensated by the energy gained by the ions [Eq. (6)].

IV. FLAT-TOP DISTRIBUTIONS

The ion orbits are easiest to analyze for flat-top electron distributions—i.e., for distributions where the electron density equals the constant $\bar{n}_0$ out to a radius $\bar{b}$, and equals zero between $\bar{b}$ and the confining wall. A typical orbit for this density profile is shown in Fig. 1. As can be seen in this figure, the diocotron frame rotating with frequency $\bar{\omega}_D$ is the most natural frame in which to analyze the orbits. The ion orbit in Fig. 1, like the orbits for most system parameters, has two important features: a slow, major oscillation around some central point and a fast, minor oscillation around the major orbit. The angular momentum variation is dominated by the major orbit.

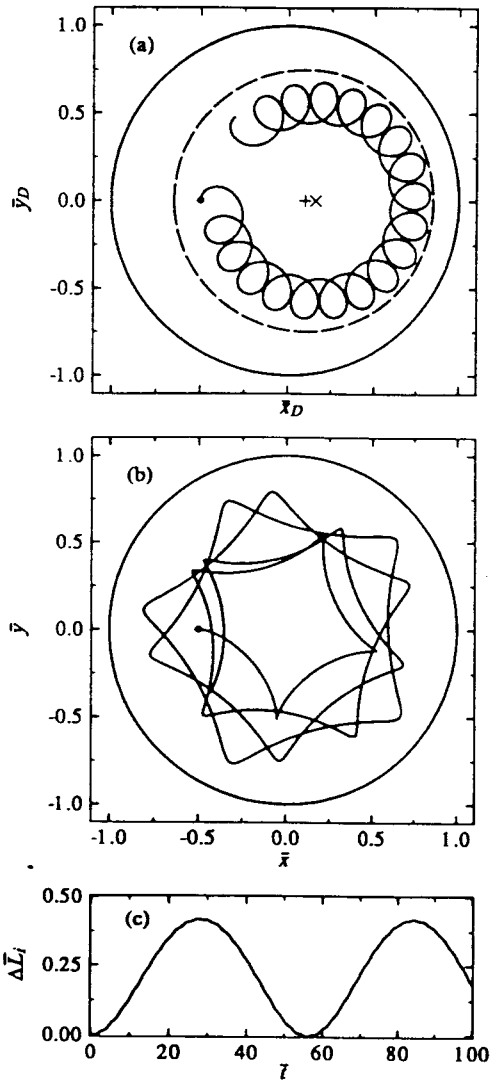

FIG. 1. The orbit of an ion of mass $m_i = 48 m_p$, for a plasma column of radius $\bar{b} = 0.75$, density $n_0 = 5.0 \times 10^7 \text{cm}^{-3}$, displaced from the origin by $\bar{R}_D = 0.1$, in a magnetic field of $B = 6500$ G. These parameters correspond to $\lambda = 1.8625$, well above resonance. In (a), the orbit is shown in the diocotron frame, and in (b) the orbit is shown in the lab frame. The solid circle is the trap wall, the dashed circle is the plasma column boundary, the + marks the center of the plasma column, the dot marks the initial ion position, and the × marks the orbit fixed point. Graph (c) shows the change in the ion angular momentum as a function of time. Note that, for clarity, the orbit in (a) and (b) is only propagated to $\bar{t} = 49.3$.

In the diocotron frame the equation of motion Eq. (3) includes centrifugal and Coriolis terms:

$$\frac{d^2\bar{x}_D}{d\bar{t}^2} = \bar{\mathbf{E}}_D(\bar{x}_D, \bar{y}_D) + \bar{\omega}_D(\lambda^{1/2} + \bar{\omega}_D)(\bar{x}_D \hat{x}_D + \bar{y}_D \hat{y}_D) + (\lambda^{1/2} + 2\bar{\omega}_D)\bar{\mathbf{v}}_D \times \hat{z}. \tag{15}$$

Since the electron column is stationary in this frame, the electric fields inside the electron column are static

$$\bar{\mathbf{E}}_D(\bar{x}_D,\bar{y}_D)=-[(\bar{x}_D-\bar{R}_D)\hat{x}_D+\bar{y}_D\hat{y}_D]$$
$$+\bar{b}^2\frac{(\bar{x}_D-1/\bar{R}_D)\hat{x}_D+\bar{y}_D\hat{y}_D}{(\bar{x}_D-1/\bar{R}_D)^2+\bar{y}_D^2}, \quad (16)$$

where the first term comes from the electron column charges and the second term comes from the image charges. Using Eq. (16), Eq. (9) reduces to

$$\frac{d\bar{L}_i}{d\bar{t}}=-\bar{y}_D\bar{R}_D(1-\bar{b}^2)+\vartheta(\bar{R}_D^2). \quad (17)$$

The change in angular momentum $\Delta\bar{L}_i$ can then be found once the values of $\bar{y}_D$ along the ion orbit are known.

A. Nonresonant behavior

Equation (15) has a fixed point at $\bar{y}_D = 0$,

$$\bar{x}_D=\bar{x}_f=\frac{1-\bar{b}^2}{1-\bar{b}^2-\bar{b}^4/\lambda}\bar{R}_D+\vartheta(\bar{R}_D^3), \quad (18)$$

and $\bar{\mathbf{v}}_D = 0$. The condition $g(\lambda_r) = 0$ defines the resonant value λ_r, where the resonant factor g is defined to be

$$g=1-\bar{b}^2-\bar{b}^4/\lambda. \quad (19)$$

Levy *et al.*[1] find maximum gain at $\lambda = \lambda_r$. Note that $\bar{x}_f = 0$ when $\lambda=0$, $\bar{x}_f \to -\infty$ when $\lambda \to \lambda_r^-$, $\bar{x}_f = \bar{R}_D$ when $\lambda=\infty$, and $\bar{x}_f \to \infty$ when $\lambda \to \lambda_r^+$. However, the fixed point becomes unphysical when significantly displaced from the electron column center.

The equation of motion (15) is simplified by transforming to a frame centered at the fixed point and rotating with frequency $\bar{\omega}_s = -h$, where

$$h=\tfrac{1}{2}\lambda^{1/2}(1+2\bar{b}^2/\lambda). \quad (20)$$

In this "spring" frame, the equation of motion reduces to the simple harmonic oscillator equation $d^2\bar{r}_s/d\bar{t}^2 = -k\bar{r}_s$, where $k = g + h^2 = 1 + \lambda/4$, and $\bar{r}_s$ is the distance to the fixed point. Assuming that the ion is initially at rest in the lab frame, the orbit in the spring frame can be found by matching the transformed initial conditions to the appropriate sinusoidal oscillations. Transforming back to the diocotron frame yields the ion orbit,

$$\bar{y}_D=-A\sin\sqrt{k}\bar{t}\sin h\bar{t}-B\cos\sqrt{k}\bar{t}\sin h\bar{t}$$
$$+C\sin\sqrt{k}\bar{t}\cos h\bar{t}+D\cos\sqrt{k}\bar{t}\cos h\bar{t}, \quad (21)$$
$$A=-\frac{\lambda^{1/2}}{2\sqrt{k}}\bar{y}_0, \quad B=\bar{x}_0-\bar{x}_f,$$
$$C=\frac{1}{\sqrt{k}}\left(\frac{\lambda^{1/2}}{2}(\bar{x}_0-\bar{x}_f)-\bar{\omega}_D\bar{x}_f\right), \quad D=\bar{y}_0, \quad (22)$$

where $(\bar{x}_0,\bar{y}_0)$ is the initial position of the ion in the lab frame.

Integration of Eq. (17) along the orbit specified by Eq. (21) gives one instance of the change in angular momentum $\Delta\bar{L}_i$. We need, however, the value of $\Delta\bar{L}_i$ averaged over all ions. Differences in $\Delta\bar{L}_i$ arise from different ion initial positions and from varying ion transit times. The average over the ion initial positions $(\bar{x}_0,\bar{y}_0)$ is straightforward; $\langle(\bar{x}_0,\bar{y}_0)\rangle = (\bar{R}_D,0)$. Consequently $\langle A\rangle=\langle D\rangle=0$. Although the average ion transit time is τ, variations in the initial $\hat{z}$ velocities and positions cause individual ions to exit the system at randomly distributed times $\bar{\tau}_e$. Integration and averaging of Eq. (21) yields terms of the form

$$\left\langle\left[\frac{\cos(\sqrt{k}\pm h)\bar{t}}{\sqrt{k}\pm h}\right]_{\bar{t}=0}^{\bar{\tau}_e}\right\rangle_{\bar{\tau}_e}. \quad (23)$$

Because the average of a sinusoid is zero, the upper limit of these terms average out. Only the lower limit contributes to the average change in $\Delta\bar{L}_i$. The surviving terms yield

$$\frac{d\bar{R}_D}{dt}=\frac{\bar{n}_i}{\bar{n}_0\tau}\frac{1-\bar{b}^2}{\lambda^{1/2}g}[(\bar{x}_f-\bar{R}_D)(h+\lambda^{1/2}/2)+\bar{\omega}_D\bar{x}_f]. \quad (24)$$

Note that the right-hand side is always positive; consequently $\bar{R}_D$ grows for *all* values of λ. Since $\bar{x}_f$ is proportional to $\bar{R}_D$, all the terms on the right-hand side are linearly proportional to $\bar{R}_D$ and the diocotron radius will increase exponentially. The growth rate diverges as λ approaches resonance, but, as shown in Sec. IV B–IV D, different expressions are required close to resonance.

The above algebra conceals a simple physical explanation for the diocotron growth. Although the ions follow complicated, cycloidal orbits, the important physics is preserved by the simplifying assumption that the ions orbit the fixed point along perfectly circular paths. The periods of all the orbits are equal. We need to average over all the initial ion positions; we can do this by following the motion of the circular cloud of ions, which, at $\bar{t} = 0$, exactly covers the electron column. As time progresses, this cloud will pivot around the fixed point. Since the fixed point is displaced from the electron column center, the cloud will generally not overlap perfectly with the electron column. For small λ (i.e., $\lambda < \lambda_r$), the ions orbit in the clockwise direction, and the fixed point is to the left of the column center ($\bar{x}_f < \bar{R}_D$). Thus the ion cloud's average initial velocity is downwards (in the $-\hat{y}$ direction). For large λ, the ions orbit with the opposite sense (counterclockwise). The fixed point shifts as well, and is now to the right of the column center ($\bar{x}_f > \bar{R}_D$). Consequently, the ion cloud's average initial velocity is still downwards. The ion cloud's average motion is well represented by the motion of an ion that is initially at the electron column center. Symmetry dictates that the electric field $\bar{\mathbf{E}}_D$ at the position of this "average ion" must be zero at $\bar{t} = 0$. Using Eq. (9), $d\bar{L}_i/d\bar{t}$ is initially zero as well. If $\bar{R}_D \ll 1$, it is easy to see that the dominant electric field is from the electron column rather than from its image. This field points radially inwards. Since the average ion initially moves downwards, then $\bar{\mathbf{x}}_D \times \bar{\mathbf{E}}_D$ must initially be positive, so from Eq. (9) $d\bar{L}_i/d\bar{t}$ must also be positive. We know from Fig. 1(c) that the change in the ion angular momentum $\Delta\bar{L}_i$ has the functional form of a biased sinusoid. The simplest such function which satisfies the above conditions on $d\bar{L}_i/d\bar{t}$ and also satisfies $\Delta\bar{L}_i(\bar{t} = 0) = 0$ is $\Delta\bar{L}_i \propto 1 - \cos\Omega t$. Since the time averaged value of $\Delta\bar{L}_i$ is always positive, the instability grows for all values of λ.

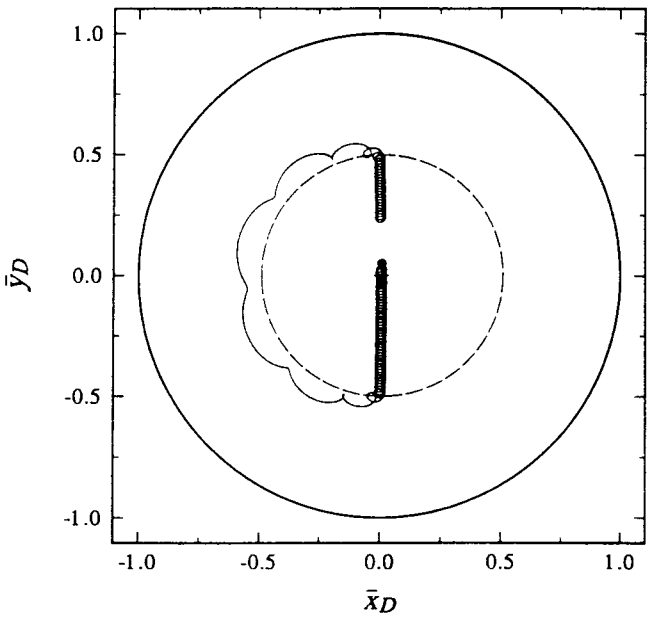

FIG. 2. The orbit, in the diocotron frame, of an ion at resonance. The plasma column radius is $\bar{b} = 0.5$, and the column is displaced from the origin by $\bar{R}_D = 0.01$. The magnetic field is $B = 1374.9$ G, corresponding to $\lambda = \lambda_r = 0.083\,33$, and the ion is propagated for $\bar{t} = 247$. All other parameters, curves, and marks are as in Fig. 1.

B. Resonance behavior for complete orbits

Near the resonance ($g \approx 0$) the fixed point is outside the plasma and the above analysis is inappropriate. Exactly on resonance ($g=0$) the velocity-independent components of the force on the ions [Eq. (15)] are particularly simple in the diocotron frame, and reduce to an effective "electric" force:

$$\begin{aligned}\mathbf{E}_{\text{eff}} &= \bar{R}_D(1-\bar{b}^2)\hat{x}_D + \vartheta(\bar{R}_D^2) && \bar{r}_D \leqslant \bar{b}, \\ &= \frac{\bar{r}_D^2-\bar{b}^2}{\bar{r}_D^2}\bar{r}_D\hat{r}_D + \bar{R}_D(1-\bar{b}^2)\hat{x}_D + \vartheta(\bar{R}_D^2) && \bar{r}_D > \bar{b}.\end{aligned} \tag{25}$$

The ions are also subject to an effective "magnetic" field $\bar{\mathbf{B}}_{\text{eff}} = 2h$, which reduces to $\bar{\mathbf{B}}_{\text{eff}} = 2$ exactly on resonance. As shown in Fig. 2, the ions $\bar{\mathbf{E}}_{\text{eff}} \times \bar{\mathbf{B}}_{\text{eff}}$ drift in these fields. Inside the plasma the ions drift downwards with velocity

$$\bar{\mathbf{v}}_{D\text{res}} = (1-\tfrac{1}{2}\bar{b}^2)\bar{R}_D\hat{y}_D. \tag{26}$$

Outside the plasma, the ions complete their orbit by returning to the top of the plasma in a clockwise arc. The equation of motion along this return arc resembles a driven inverted pendulum equation. For ions that start at the center of the electron column, the average change induced in the diocotron radius is

$$\Delta\bar{R}_{D\text{cen}} = \frac{(1-\bar{b}^2)^{1/2}}{3\bar{R}_D} + \frac{1}{3}\left(\frac{2\pi}{\bar{R}_D}\right)^{1/2}(1-\bar{b}^2) + \vartheta(\bar{R}_D^0), \tag{27}$$

where the first term is the exact contribution from the downward ion motion inside the plasma and the second term is the approximate contribution from the return arc.

The change in $\bar{R}_D$ induced by ions born away from the column center is generally lower than that predicted by Eq. (27). However, $\Delta\bar{R}_{D\text{cen}}$ is a good indicator of the average change in $\bar{R}_D$ for all ions. Using the numerical simulations presented in Sec. V, I find, to a good approximation, that the spatially average angular momentum change is related to the change for a centered particle by the formula $\langle\Delta\bar{R}_D\rangle = 1.5(\bar{R}_D^{0.188}/\bar{b}^{0.307})\Delta\bar{R}_{D\text{cen}}$, yielding an on resonance growth rate of

$$\frac{d\bar{R}_D}{dt} = \frac{1}{2}\frac{\bar{n}_i}{\bar{n}_0\tau}\frac{R_D^{0.188}}{\bar{b}^{0.307}}\left[\frac{(1-\bar{b}^2)^{1/2}}{3\bar{R}_D} + \frac{1}{3}\left(\frac{2\pi}{\bar{R}_D}\right)^{1/2}(1-\bar{b}^2)\right]. \tag{28}$$

The diocotron radius increases roughly as $\bar{R}_D \propto \bar{t}^{(0.55)}$.

C. Resonance behavior for incomplete orbits

Equation (28) is inapplicable when the diocotron radius $\bar{R}_D$ is very small or when the transit time $\bar{\tau}$ is very short. In these situations the ions do not have time to completely traverse the electron column and, consequently, do not execute complete orbits. Instead, the ions simply drift steadily downwards with velocity $\bar{\mathbf{v}}_{D\text{res}}$. Using Eq. (17) and the result $h \approx 1$ at resonance, the change in the angular momentum for a typical ion is

$$\begin{aligned}\Delta\bar{L}_i &= [(\bar{y}_D - \bar{\mathbf{v}}_{D\text{res}}\bar{t})^2 - \bar{y}_D^2]_{\bar{t}=0}^{\bar{\tau}_e} \\ &= 2\bar{y}_D\bar{\mathbf{v}}_{D\text{res}}\bar{\tau}_e + \bar{\mathbf{v}}_{D\text{res}}^2\bar{\tau}_e^2.\end{aligned} \tag{29}$$

Because $\langle\bar{y}_D\rangle = 0$, only the second term contributes to the spatial average, and using Eqs. (13) and (26), the diocotron radius increases as

$$\frac{d\bar{R}_D}{dt} = \frac{\bar{n}_i}{\bar{n}_0\tau}(1-\bar{b}^2)^{2.5}\frac{\langle\bar{\tau}_e^2\rangle}{4\bar{b}^2}\bar{R}_D, \tag{30}$$

where $\langle\bar{\tau}_e^2\rangle$ is the mean square transit time. Under these conditions the diocotron radius increases exponentially.

D. Resonance behavior for ejected orbits

The results of the previous sections are valid only when the ion orbits are either regular or stay inside the electron column. When the diocotron radius $\bar{R}_D$ is large, many ions leave the electron column, and may then execute highly irregular orbits. Ultimately these ions hit the outer cylindrical wall. Since the energy of the ions scales with the potential drop across the electron column, the velocity of a typical ion under these conditions scales as $\bar{\mathbf{v}} \approx \bar{b}$; consequently its angular momentum at the wall is also on the order of $\bar{b}$. Near resonance, $\bar{b}^2/\lambda^{1/2} \approx 1$, so Eq. (14) becomes

$$\frac{d\bar{R}_D}{dt} \approx \frac{1}{2}\frac{\bar{n}_i}{\bar{n}_0\tau}\frac{1}{\bar{b}\bar{R}_D}, \tag{31}$$

where the factor of 1/2 comes from numerical simulations. Here the diocotron radius increases with $\sqrt{t}$.

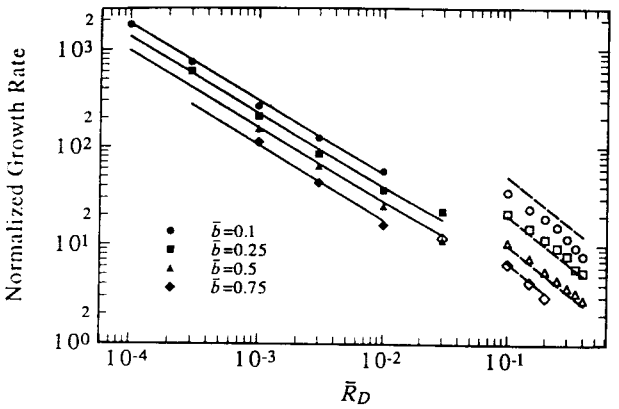

FIG. 3. The normalized growth rate $(\bar{n}_0\tau/\bar{n}_i)d\bar{R}_D/dt$ versus the diocotron radius $\bar{R}_D$. The solid symbols are the results of the numerical simulations, and the lines are calculated from the theory as described in the text. The hollow symbols correspond to orbits where the ions hit the wall. Here λ is adjusted for maximum growth, and τ is adjusted to ensure that the ions undergo complete orbits.

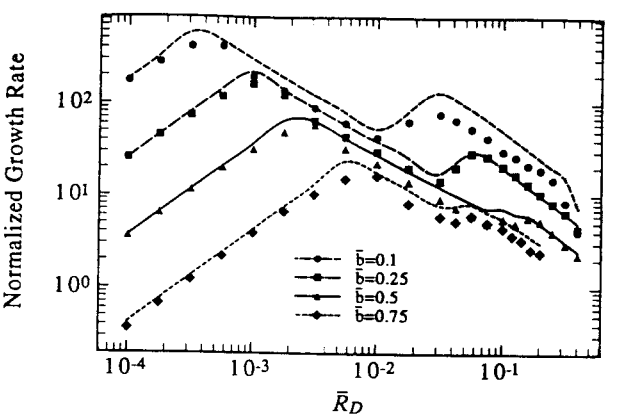

FIG. 4. The normalized growth rate $(\bar{n}_0\tau/\bar{n}_i)d\bar{R}_D/dt$ versus the diocotron radius $\bar{R}_D$. The solid symbols are the results of the numerical simulations, and the lines are calculated from the theory as described in the text. Here λ is set to λ_r for each curve, and the orbits are propagated out to $\tau=500$ μsec. Ions of mass $m_i = 48m_p$ are used, and the electron column density is $n_0 = 2.75 \times 10^7 \text{cm}^{-3}$.

When the column radius $\bar{b}$ is large, the ejected ion orbits resemble the complete resonant orbits of Sec. IV B. up to the point where the ejected ions hit the wall. However, since the ejected ions hit the wall at a point at which their angular momentum change is nearly maximum, these ions couple angular momentum to the electron column more efficiently than the ions undergoing complete resonant orbits.

V. NUMERICAL CALCULATIONS

The above expressions for $d\bar{R}_D/dt$ [Eqs. (24), (28), (30), and (31)] are based on various simplifications. A numerical code was developed to confirm the validity of these simplifications and to find the growth rates in the transition regions. The code integrates the ion equation of motion Eq. (3) to find the orbit of each ion for a time $\bar{\tau}$. A large number of ions are followed, with each ion starting from a different position in the electron column. If the ion does not hit the wall, each ion is assumed to transfer to the electron column its average angular momentum change. The average angular momentum change is used instead of the change at precisely $\bar{t} = \bar{\tau}$ because of the randomness in the exit times $\bar{\tau}$. When the ion does hit the wall, it generally hits in a time much less than the exit time $\bar{\tau}$. In this case, the full angular momentum possessed by the ion when it hits the wall is transferred to the electron column.

A. Flat-top distributions

Figure 3 shows the maximum growth rate vs the diocotron radius $\bar{R}_D$ for several values of $\bar{b}$. In all cases the exit time $\bar{\tau}$ was adjusted to allow the ions to execute complete orbits, and λ was scanned for the maximum growth. For small $\bar{R}_D$ the growth rate follows the prediction of Eq. (28) for roughly square root growth. The value of λ which yields maximum growth slowly increases away from the resonant value λ_r as $\bar{R}_D$ is increased. For large $\bar{R}_D$, the ions hit the wall and the growth rate follows the prediction of Eq. (31); the values of λ that yield maximum growth are substantially different from and can be greater or less than λ_r.

Experimentally, the maximum growth rates shown in Fig. 3 are never realized. Not only are the exit times constrained to some maximum value as discussed in Sec. III, but, since the instability grows from noise, the value of λ remains unchanged at some value very near the resonant value λ_r. The resonant growth rate versus the diocotron radius $\bar{R}_D$ is shown in Fig. 4. All curves follow the same pattern as the diocotron radius $\bar{R}_D$ is increased: exponential growth at small $\bar{R}_D$ corresponding to the incomplete orbits of Sec. IV C, approximately square root growth corresponding to the complete orbits of Sec. IV B, linear to quasiexponential growth in a transition region, and approximately square root growth at-large $\bar{R}_D$ corresponding to the ejected orbits of Sec. IV D. Where there are no ejected orbits, the theory curves are calculated with either Eq. (30) or Eq. (28), where the choice between the two equations is based on which equation's validity range is more appropriate. [Remember that Eq. (30) is valid for small $\bar{R}_D$, while Eq. (28) is valid for somewhat larger $\bar{R}_D$.] This choice is equivalent to using the smaller of the growth rates predicted by the two equations. When some of the ions are ejected, the theory curves are calculated by finding the appropriate weighted average of Eqs. (28) and (31) where the weights are derived from the numerically determined number of ejected orbits.

Figure 5 shows the growth rate versus λ for two values of $\bar{R}_D$. The theoretical curves were found as described for Fig. 4. The fastest growth occurs for a fairly broad range of λ near λ_r. The growth rate steadily declines for high values of λ, but growth persists at a reduced level even as λ approaches zero. Because of the large number of ejected orbits, fast growth occurs over a wider range of λ for large $\bar{R}_D$ than for small $\bar{R}_D$.

Figure 6 shows the diocotron radius $\bar{R}_D$ versus $\bar{t}$ for λ on resonance and for λ far from resonance. On resonance,

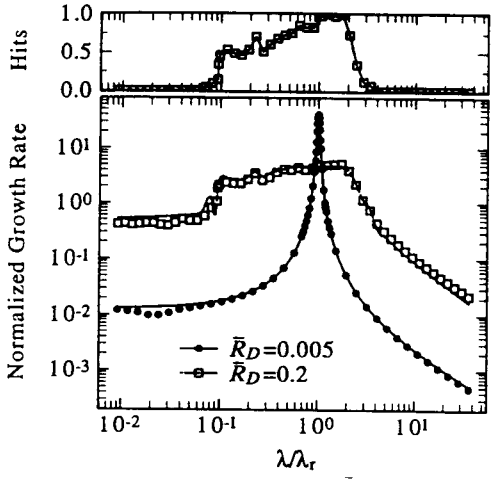

FIG. 5. The normalized growth rate $(\bar{n}_0\tau/\bar{n}_i)d\bar{R}_D/dt$ versus λ/λ_r, for a flat-top electron density distribution. The dots are the results of the numerical simulations, and the lines are calculated from the theory as described in the text. The upper graph shows the fraction of ejected ions for the $\bar{R}_D = 0.2$ curve. No ions are ejected for $\bar{R}_D = 0.005$. The column radius is $\bar{b} = 0.53$, and the other graph parameters are given in Fig. 4.

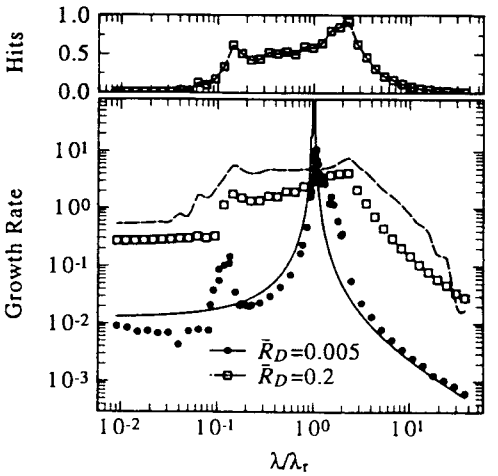

FIG. 7. The normalized growth rate $(\bar{n}_0\tau/\bar{n}_i)d\bar{R}_D/dt$ versus λ/λ_r, for a parabolic electron density distribution. The graph parameters are the same as those in Fig. 5.

$\bar{R}_D$ is initially proportional to the square root of $\bar{t}$, but soon grows linearly with $\bar{t}$. Far from resonance $\bar{R}_D$ grows exponentially.

B. Non-flat-top density distributions

The flat-top distributions used above cannot be obtained experimentally. Realistic electron column density distributions will have rounded edges and need not be monotonic. In Fig. 7, I show the growth rate versus λ for the parabolic density distribution $f(u) = 1 - u^2/2$ for $u < \sqrt{2}$, $f(u)=0$ elsewhere. Figure 7 is very similar to Fig. 5, which shows the same curves for a flat-top distribution. The major differences between these two graphs are that the growth rate is broader and slightly smaller for the parabolic distribution. These changes can be understood by realizing that different initial ion radii are in resonance at slightly different values of λ. The small peak at small λ is not understood, and may be a numerical artifact. In general, parabolic density distributions (and, presumably, other non-flat-top density distributions) behave qualitatively the same as flat-top density distributions.

One of the most striking features of the experimental observations of this instability is that the instability grows linearly at all observable amplitudes for many system parameters. While linear growth is obtained by the simulation for flat-top distributions only at large amplitudes (Fig. 6), linear growth can be obtained with a parabolic density distribution (Fig. 8) at all experimentally observable amplitudes. Along with the simulation result, Fig. 8 also

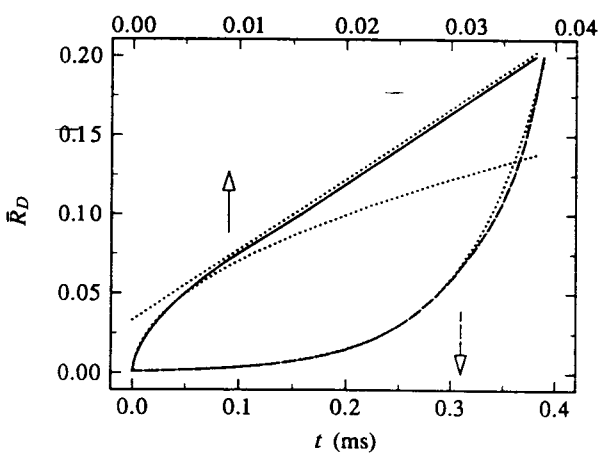

FIG. 6. The diocotron radius $\bar{R}_D$ versus time, for a flat top electron distribution. The solid curve shows on-resonance growth ($\lambda = \lambda_r = 0.1097$), and the appropriate time scale is found along the upper horizontal axis. The dashed curve shows off-resonance growth ($\lambda = 0.009\,88$), and the appropriate time scale is found along the lower horizontal axis. The dotted lines are reference curves showing perfect linear, square root, and exponential growth. The ion fractional density is $n_i/n_0 = 1.6 \times 10^{-4}$, and the other graphs parameters are the same as those in Fig. 5.

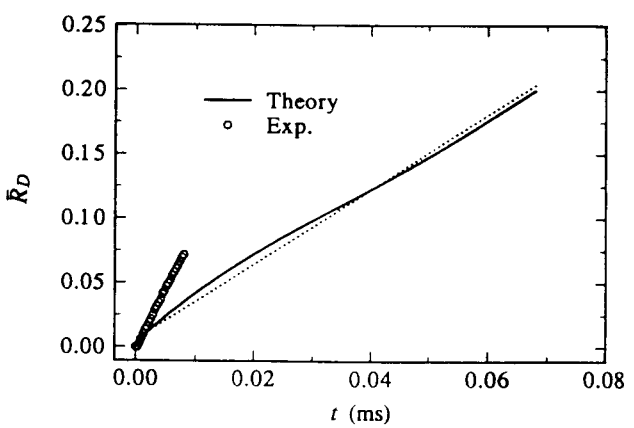

FIG. 8. The diocotron radius $\bar{R}_D$ versus λ/λ_r, for a parabolic distribution. The solid curve is from simulation, and the circles are from the experiments of Peurrung *et al.*[6] The dotted line is a reference line showing perfect linear growth. The other graph parameters are the same as those in Fig. 6.

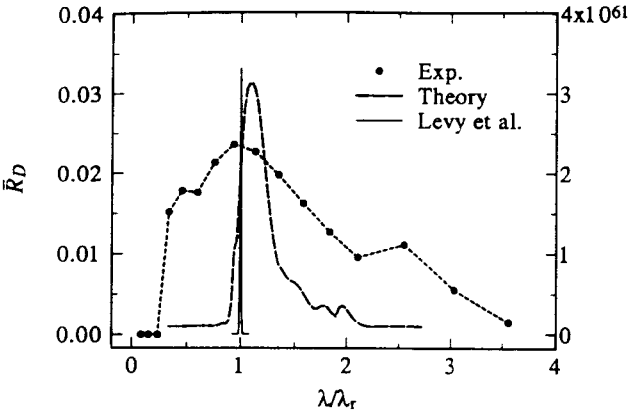

FIG. 9. The diocotron radius $\bar{R}_D$ versus λ at time $t=14.3$ msec. The diocotron radii predicted by the simulation and measured in the experiment refer to the scale on the left vertical axis. The diocotron radii predicted by Levy *et al.* refer to the scale on the right vertical axis, and are obviously unphysical. The electron column density is $n_0 = 3.2 \times 10^7\ \mathrm{cm}^{-3}$, the column radius is $\bar{b} = 0.49$, and a parabolic density distribution is used in the simulations. All other parameters are the same as in Fig. 6.

shows the experimental growth curve[6] corresponding to the simulation parameters. The theoretical growth rate obtained from the simulation is half as large as the experimentally observed growth rate.

Figure 9 displays the experimentally[6] and theoretically obtained diocotron amplitude $\bar{R}_D$, at the fixed time $t=14.3$ msec, as a function of λ. While the maximum growth rates are comparable, the width of the calculated growth region is significantly less than the width of the experimentally measured growth region. Note, however, that the large amplitude growth curves shown in Figs. 5 and 7 are broader than the experimental curve shown here. For reference, I have also included the amplitude predicted by Levy *et al.* for these parameters.

VI. DISCUSSION

Given the experimental uncertainties (in determining m_i, τ, n_0, and the spatial electron density distribution), the qualitative behavior and the growth rates predicted by the transient ion resonance instability theory presented in this paper are in good agreement with the experimental measurements reported by Peurrung *et al.*[6] The only fitted parameter used in any of these comparisons is the ion mass m_i, which is found by fitting λ_r to the experimentally determined magnetic field that yields maximum growth. Thus there are no independent parameters available to be used to fit the growth rates. Levy *et al.*'s theory for trapped ions, on the other hand, is clearly incorrect in this situation (see the Appendix).

There are two important discrepancies between the transient ion resonance theory presented here and the experimental results. First, while linear growth ($\bar{R}_D \propto t$) is found experimentally for almost all experimental parameters, it is not found theoretically for such a wide range of parameters. Note, however, that the exponential growth observed theoretically for small growth rates far from resonance are also occasionally observed experimentally very far from resonance. Second, the experimentally observed growth region is broader than theoretically predicted. The explanation of this discrepancy might simply be that more than one ion species participates in the experimental instability. This would lead to two or more resonant values of λ, and appropriately broadened curves. If, however, only one species participates, we need a more subtle explanation of the peak broadening. Inspection of Fig. 4 shows that growth is linear and very broad in the regime where an increasing fraction of the ions are lost to the wall. The two discrepancies mentioned above may be the result of some mechanism that causes ions to be ejected into the wall earlier than expected. An alternate explanation may come from a mechanism that causes the ions to leave the plasma column at a preferential orbit phase. Remember that shielding from the electron column prevents the ions from being accelerated in the $\hat{z}$ direction. Because the electron column center and the ion fixed point do not coincide, a portion of the orbit for some fraction of the ions is outside the electron column. Shielding ceases when the ions leave the electron column radially, and such ions are accelerated to the plasma column end. This mechanism might lead to a disproportionate fraction of the ions passing out of the system while radially outside the column. If this were to occur, the averaging procedures used throughout this paper would be invalid and, since the ion's angular momentum along the orbit is maximized outside the electron column, the calculated growth rate would increase.

Since many of the current pure electron plasmas traps satisfy, or are close to satisfying, the resonance condition $\lambda_r = \bar{b}^4/(1-\bar{b}^2)$,[10,13–15] the ion resonance instability can occur in these machines if the electron temperature is sufficient to cause ionization. Parameter ranges exist in which positron–antiproton and cryogenic electron (with a hot tail) plasmas would be unstable. However, the instability can easily be stabilized with negative feedback.[16,10] The resonance condition would not be satisfied in an electron plasma containing positrons for any plausible set of parameters. However, the transient ion resonance theory considered here is inapplicable in this case because the character of the positron orbits under these conditions is so different from that of the ion orbits. Mechanisms exist to destroy such a plasma; for instance, analogous to the behavior of two near and oppositely signed vortices, a plasma consisting of equally charged, slightly displaced, electron and positron columns would immediately flow into the trap wall.

Finally, I have briefly considered the effect of negative ions on the ion resonance instability. Such ions can be created by electron attachment reactions. In this situation the right-hand side of Eqs. (6) and (9) changes sign. Negatively charged ions are untrapped by the electron plasma column, so the orbits for such ions are quite different from the orbits of positive ions. Preliminary numerical studies indicate that the presence of negative ions causes the diocotron radius to decrease. Of course, a positron plasma[17] contaminated with negative ions would be completely equivalent to the normal situation.

ACKNOWLEDGMENTS

I thank John Notte, Anthony Peurrung, Ralph Smith, and members of the University of California, San Diego pure electron plasma group.

This work was supported by Office of Naval Research and the National Science Foundation.

APPENDIX: EFFECT OF INITIAL CONDITIONS ON LEVY'S *ET AL*'S THEORY

Levy *et al.*[1] found the growth rate for the ion resonance instability when the ions are trapped. The result of their work is a dispersion relation [their Eq. (59)] that predicts growth in a narrow region around $\lambda = \lambda_r$. Since their calculation employs Fourier transforms, they ignored the effect of initial conditions. Using Laplace transforms instead, their work can be trivially extended to yield

$$\mathcal{L}\{E_\theta(x)\} = -\frac{i/[\omega_e(1-x_D)]}{1-(1-x)/(1-x_D)-\alpha\lambda(1-x)/(\lambda-\lambda x-x^2)} \times E_\theta(t=0), \tag{A1}$$

where $\mathcal{L}\{E_\theta\}$ is the Laplace transform of the azimuthal electric field, x is the normalized frequency $x = \omega/\omega_e$, $\omega_e = en_0/2\epsilon_0 B$ is the rotation rate of the electron column, $x_D = \bar{b}^2$ is the normalized diocotron frequency, and α is the fractional neutralization of the electron column. I have allowed for an initial field $E_\theta(t = 0)$ produced by a perturbation on the electrons only. Levy *et al.* model the instability as a surface wave; E_θ is equivalent to the diocotron radius R_D.

The Laplace transform in Eq. (A1) can be inverted by the standard residue method. While the dispersion relation associated with Eq. (A1) is cubic, near resonance only the two complex conjugate roots are important, and the solution is approximately $E_\theta(t) = E_\theta(0)\cosh(\Gamma T)$, where $\Gamma = \omega_e\,\mathrm{Im}(x)$ is the growth rate. For the parameters of Fig. 8, $\Gamma = 9.1 \times 10^3 \mathrm{sec}^{-1}$.

While Levy *et al.*'s theory was developed for trapped ions, untrapped ions that escape in a time τ can be modeled as follows: Imagine depositing an unbunched ion "slug" in the trap. Allow the instability to grow for time τ, and then completely remove the ion slug, leaving the electrons bunched as appropriate for the current instability amplitude. Next deposit another unbunched ion slug and repeat. This somewhat ad hoc procedure yields

$$\begin{aligned} E_\theta(t) &= E_\theta(0)(\cosh\Gamma\tau)^{t/\tau} \\ &= E_\theta(0)\exp(\Gamma^2\tau t/2), && \Gamma\tau \ll 1, \\ &= E_\theta(0)\exp[\Gamma t-(t/\tau)\ln 2], && \Gamma\tau \gg 1. \end{aligned} \tag{A2}$$

Clearly the minimum growth rate $\Gamma_{\min}$ is close to the minimum of Γ and $\Gamma^2\tau/2$, which equals Γ for the parameters of Fig 8.

Because there exists a maximum amount of angular momentum that each ion can contribute to the electron column, it is easy to establish that this model saturates at a very small diocotron radius. If I take this maximum amount to be the angular momentum of an ejected ion, then the maximum possible growth rate is given by Eq. (31). For exponential growth with growth rate $\Gamma_{\min}$, this implies that

$$\bar{R}_D < \left(\frac{1}{2}\frac{\bar{n}_i}{\bar{n}_0\tau}\frac{1}{\bar{b}\Gamma_{\min}}\right). \tag{A3}$$

For the parameters of Fig. 8, this inequality reduces to $\bar{R}_D < 0.006$. In general, for small fractional neutralizations ($\alpha \ll 1$), the diocotron radius is limited to values well below the observational threshold, and one would not expect to be able to see growth following Eq. (A2).

[1] R. H. Levy, J. D. Daugherty, and O. Buneman, Phys. Fluids **12**, 2616 (1969).
[2] R. H. Levy, Phys. Fluids **8**, 1288 (1965).
[3] C. Litwin, M. C. Vella, and A. Sessler, Nucl. Instrum. Methods **198**, 189 (1982).
[4] A. Wolf, Phys. Scr. **T22**, 55 (1988).
[5] T. E. Cowan, R. H. Howell, and R. R. Rohatgi, Nucl. Instrum. Methods B **56**, 599 (1991).
[6] A. J. Peurrung, J. Notte, and J. Fajans, Phys. Rev. Lett. **70**, 295 (1993).
[7] J. D. Daugherty, J. E. Eninger, and G. S. Janes, Phys. Fluids **12**, 2677 (1969).
[8] W. Clark, P. Korn, A. Mondelli, and N. Rostoker, Phys. Rev. Lett. **37**, 592 (1976).
[9] P. Zaveri, P. I. John, K. Avinash, and P. K. Kaw, Phys. Rev. Lett. **68**, 3295 (1992).
[10] J. H. Malmberg, C. F. Driscoll, B. Beck, D. L. Eggleston, J. Fajans, K. Fine, X. P. Huang, and A. W. Hyatt, in *Nonneutral Plasma Physics*, AIP Conf. Proc. 175, edited by C. Roberson and C. Driscoll (American Institute of Physics, New York, 1988), p. 28.
[11] T. M. O'Neil, Phys. Fluids **23**, 2216 (1980).
[12] T. M. O'Neil (private communication, 1993).
[13] G. Rosenthal, G. Dimonte, and A. Y. Wong, Phys. Fluids **30**, 3257 (1987).
[14] R. W. Gould and M. A. LaPointe, Phys. Rev. Lett. **67**, 3685 (1991).
[15] J. Notte, A. J. Peurrung, J. Fajans, R. Chu, and J. Wurtele, Phys. Rev. Lett. **69**, 3056 (1992).
[16] W. D. White, J. H. Malmberg, and C. F. Driscoll, Phys. Rev. Lett. **49**, 1822 (1982).
[17] C. M. Surko and T. J. Murphy, Phys. Fluids B **2**, 1372 (1990).